THE JOURNAL OF PHYSICAL CHEMISTRY C

Article

Cite This: J. Phys. Chem. C 2019, 123, 16577−16587

pubs.acs.org/JPCC

Modulation, Characterization, and Engineering of Advanced Materials for Electrochemical Energy Storage Applications: MoO_3/V_2O_5 Bilayer Model System

Ran Attias,* Michael Salama,* Reeta Pant, Yossef Gofer, and Doron Aurbach*

Department of Chemistry and the Institute of Nano-Technology and Advanced Materials (BINA), Bar- Ilan University, Ramat Gan 5290002, Israel

Supporting Information

ABSTRACT: Core−shell, multilayered and coated materials have great importance to electrochemical energy storage systems, sensors, actuators, photonics, and photoactive applications. A deeper understanding of the effect of combining different materials in complex structures on their physical and electrochemical properties is vital for better engineering of such compounds and wise modulation of their physical characteristics. Herein we proposed a model system of thin film MoO_3/V_2O_5 bilayer systems. The crystallinity, texture, and morphology of each layer in the bilayer structures were determined by X-ray diffraction (XRD), Raman spectroscopy, high resolution scanning electron microscopy (HR-SEM), and atomic force microscopy (AFM). The electrochemical properties were studied via slow scan rate cyclic voltammetry (SSCV) in lithium ions containing solution. The study clearly shows that the physical and electrochemical properties of each layer in a bilayer configuration are not similar to the properties of the single material. Therefore, at least for bilayer materials, the whole structure properties are more complex than simply combining the properties of the individual materials.

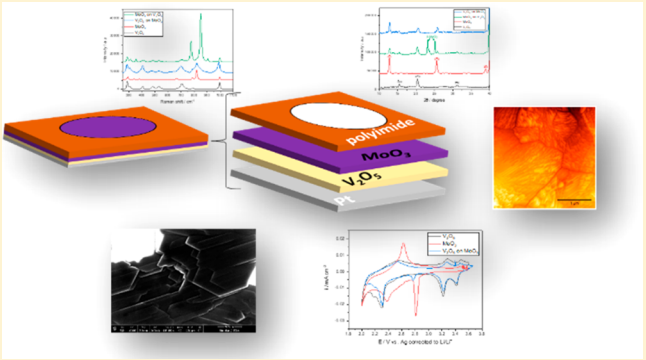

INTRODUCTION

Electrochemistry and materials science are inseparable fields. In the past few years, there are numerous articles about complex structural materials, such as core−shell,[1−16] multilayered, and coated[17−20] materials, for electrochemical,[1,2,16−20,3−6,8,9,14,15] electronic,[7,10] and photonic[11−13,21] systems. However, little is known about the effect of combining different materials in complex structures on their physical and electrochemical properties.

In particular, active electrode materials for electrochemical energy storage and conversion devices with complex structural characteristics have been of great interest in the past decade or two. The various structural virtues are expected to improve the material's properties by numerous mechanisms. It can be by imparting better stability, better chemical compatibility within electrochemical systems, high interfacial stability, useful passivation, enhanced electronic and/or ionic conductivities, and so forth. There are plenty of reports and patents that demonstrate the advantage of this approach for various electrodes, electrolytes, and complete cells.

Core−shell structures are of the most studied type of composites, intended to resolve technical problems associated, usually, with direct interaction of the active material with electrolyte solutions.[22,23] For instance, a stable artificial solid electrolyte interphase (SEI) shell or layer may isolate Li, Mg, Na, or Ca based anodes from direct reaction with the electrolyte solution, thus circumventing corrosion and deterioration of the cells.[24−28] Similar coatings may also mitigate corrosion, Mn dissolution in lithium cells, and many other issues. Core−shell structured cathode materials are also envisaged as a strategy for stabilizing high-voltage transition-metal oxides from corrosion in Mg-reversible electrolytic solutions containing chlorides. In the latter case, the shell is engineered to be good Mg ion conductor while being chemically stable with chlorides and Lewis acids. The actual mechanism of the core material stabilization as well as the ion transport through the layer are, in many cases, not fully understood. Many basic points are of great importance in understanding the mode of operation of these intricately engineered structures.

For instance, let us scrutinize the case of metal-oxide core (e.g., V_2O_5) protected by a pinhole-free, dense, monolithic thin layer of magnesium ion conductor, (e.g., Chevrel phase). The latter is stable in chlorides-based solutions supporting highly reversible magnesium deposition. In addition, for being a good Mg ion conductor, Chevrel phases are also electrochemically reactive intercalation compounds and possess electronic conductivity that varies with the intercalation level. Thus, for a Chevrel phase to transport Mg, and for that matter also Li and

Received: May 8, 2019
Revised: June 16, 2019
Published: June 17, 2019

DOI: 10.1021/acs.jpcc.9b04371
J. Phys. Chem. C 2019, 123, 16577−16587

any other ion, it has to be biased to the intercalation potential. In a simplistic manner, one can envisage this interphase mode of action as concerted intercalation and deintercalation of ions at the two interphases, solution-Chevrel and Chevrel-V_2O_5 at the same time. The actual reaction and ion transport (net) direction will depend on the electrode's bias. Thus, for both intercalation and deintercalation of the active material, the electrode must be biased to the intercalation potential of the interphase barrier material. This potential will, in this case, be appreciably lower than the intercalation potential for the core active oxide. Under the best conditions, this will entail large energy losses. A similar situation is expected to occur also with pinhole-free, nonporous carbon encapsulated electroactive materials. Obviously, the actual situation will be way more complex than that. Apart from technical considerations, like adhesion, mismatch in thermal expansions, interfacial contact, and materials' volume changes during electrochemical reactions, there are many other properties and that are not simple to predict. For instance, how would the electronic conductivity of the core (active material), and the shell (interphase), influence the electrochemical response? How do these parameters change during the changing intercalation level of the active material? How would the interfacial section between the two solid phases be like? After all, is it in fact a contact zone between two materials with different oxidation potentials, and intercalation levels? How would the electrochemical behavior of such composite systems be influenced by the changing redox potential of the active material? Of particular interest is the case when the active-material potential changes to values below and above that of the interphase-barrier layer.

Naturally, all these questions are quite complicated to predict. It is also a complicated task in the experimental realm. Deposition of monolithic, dense, pinhole-free thin layers of transition metal oxides, sulfides, and selenides are not a simple task. It is way more complicated when one considers the strict requirements for preparation of samples for electrochemical studies. For one thing, the substrate must be a good electronic conductor, electrochemically inert, and stable under the thin-layer deposition conditions. The layers must be very thin, in the several tens of nanometer thick range. The deposits must possess sufficient electronic conductivity. The material must be electrochemically active and reversible under the electrochemical studies conditions. And the deposits must be completely pinhole free, covering macroscopic layers that are manageable for electrochemical studies. Obviously, bilayers, which are the core interest, are orders of magnitude more complicated to achieve. Although metarial's crystallinity is not a prerequisite, crystalline materials, with well-defined electrochemical responses are much preferred over amorphous materials. At the same token, for results clarity, phase-transition intercalation materials are much preferred over solid-solution ones. Displacement, redox, and conversion electrochemically active materials are not of interest in the current study.

Due to the well-established difficulties with Mg intercalation mechanisms, it would have been of greatest interest to study such bilayer structured composites with Mg ions. However, embarking on such an intricate study with a notoriously convoluted Mg ion electrochemical system makes little sense. Thus, in the following study, we used lithium ions for the electrochemical experiments as a first stage, although the two solid-state materials had been shown to intercalate reversibly magnesium ions also.[29]

Practical composite structures of this kind for battery utilization will, most probably, be particulate matter, namely core−shell powder. However, for scientific studies, flat, highly controlled, simple bilayers have many advantages. It greatly simplifies the utilization of various analyses methods, such as electrochemical, structural, crystallographic and spectroscopic. Although definitely not trivial, it improves the likelihood of obtaining appropriate structured samples possessing the critical properties mentioned above. In this paper, we present the first set of experiments in the quest for studying the physical properties of simple bilayers made of two well-studied intercalation compounds, V_2O_5 and MoO_3. Some fundamental properties of the bilayers were investigated by powder X-ray diffraction (XRD), Raman spectroscopy, high-resolution scanning electron microscopy (HR-SEM), atomic force microscopy (AFM), and cyclic voltammetry. This study provides valuable scientific insights related to some of the factors that should be taken into account when conducting research with such systems.

METHODS

Materials. $LiClO_4$ (ACS reagent grade), MoO_3 powder, and 99.8% acetonitrile (ACN) were purchased from Sigma-Aldrich. V_2O_5 chunks were obtained from Kurt J. Lesker. Carbon cloth (507-20 type) with high surface area of 2000 $m^2\ g^{-1}$ was purchased from Kynol.

The materials for electrochemical experiments were dried, as following. $LiClO_4$ and activated carbon cloth (AC) were dried under dynamic vacuum for 48 h at 140 and 100 °C respectively. Solvents were dried with 4 Å activated molecular sieves.

All the electrochemical measurements, sample preparations, materials and, solutions were carried out in Ar-filled glovebox (MBRAUN), with less than 1 ppm water and oxygen levels.

Thin Film Deposition. Bilayer structures of MoO_3/V_2O_5 and V_2O_5/MoO_3 of around 20 nm (each layer) were thermally deposited from pure V_2O_5 chunks and MoO_3 powder on 1 cm^2 Pt current collectors. The deposition process was conducted under dynamic vacuum of 2×10^{-4} Torr. The first layer was deposited on a round area with 6 mm diameter at the center of the Pt electrode, the second layer was deposited on top of all electrode area (1 cm^2). To prevent a situation in which the same material form two different interfaces (i.e., material−current collector and material−solution), the electrodes were covered with the electronic insulator polyimide (Kapton) not including a round area of 0.07 cm^2 at the middle of the electrode. Configuration ensured the majority of the outer material did not touch the current collector, and the majority of the inner material did not form interface with the electrolyte solution.

After each evaporation cycle, the deposit material was annealed. The V_2O_5 film was annealed at 450 C° for 4.5 h, and MoO_3 film was annealed at 360 C° for 2 h. Single layered thin films of MoO_3 and V_2O_5 were also prepared in the same procedure as control systems.

Electrochemical Measurements. All electrochemical measurements were conducted in a three electrode cell setup, composed of a working electrode (WE), Ag wire reference electrodes (RE), and AC counter (CE) in 0.25 M $LiClO_4$/ACN electrolyte solution using multipotentiost/galvanostat channel instruments (VMP-3 potentiostat, Bio-Logic Co.).

Ag wire was examined as reference electrode using two compartment cell configuration connected by salt bridge. One half cell was composed of Pt counter and working electrode in

DOI: 10.1021/acs.jpcc.9b04371
J. Phys. Chem. C 2019, 123, 16577−16587

0.25 M $LiClO_4$ + 0.05 M ferrocene/ACN while the second half cell was composed of Ag wire reference electrode in 0.25 M $LiClO_4$/ACN electrolyte solution. Sequences of cyclic voltammetry and open circuit potential measurements were applied over 48 h, and the redox peaks of the ferrocene/ferrocenium redox couple were recorded. The Ag wire was found to be a stable quasi-reference electrode in this electrolyte solution. The Ag potential was found to be 3.1 V vs Li/Li^+ (±60 mV).

$LiClO_4$/ACN was chosen as the electrolyte solution due to the anodic stability of the perchlorate anion and the acetonitrile solvent.[30] In addition, this system allows a relatively facile intercalation process without complicated interfacial issues.

Characterizations. The crystalline structure and the texture of the thin film electrodes were determined by X-ray diffraction measurements using the AXS D8 Advance diffractometer from Bruker, Inc. in the 2θ range from 10° to 42°, with a step size of 0.03, at a rate of 10 s per step.

Further structural and phase determinations were carried out via vibrational spectroscopy using Raman spectroscopy (JY Horiba spectrometer with a He−Ne 632.817 nm laser, high-density grating). A silicon wafer was used for calibration before and after every set of measurements (using the major peak at 520.7 cm^{-1}).

Chemical analysis and morphology investigation were carried out by energy-dispersive X-ray spectroscopy (EDAX), HR-SEM (FEI, Magellan 400L), and atomic force microscopy (AFM).

The AFM measurements were carried out using a Bio FastScan scanning probe microscope (Bruker AXS). All images were obtained using soft tapping mode with a Fast Scan B (Bruker) silicon probe (spring constant of 1.8 N/m). The resonance frequency of the cantilever was approximately 450 kHz (in air). The measurements were performed under environmental conditions. The images were captured in the retrace direction with a scan rate of 1.6 Hz. The resolution of the images was 512 samples/line. Nanoscope Analysis software was used for image processing and roughness analysis. Before roughness analysis of the images, the "flatting" and "planefit" functions were applied to each image.

RESULTS AND DISCUSSION

Materials Crystalline Structure Analysis. Thin film deposition is a very rich and varied field. In the study of thin films, many important properties of the obtained materials are of interest. One of the greatest parameters pertaining to the electrochemical properties of the film is its crystalline structure. The crystalline structure (and order) of thin deposited films are strongly influenced by a host of parameters, even for a single deposition technique. Hence, the influence of the deposition conditions on the material's properties is extremely valuable. There are numerous publications reporting and elucidating these effects in great detail. Unfortunately, there are very few papers dealing with multilayers of very thin, electrochemically active materials, deposited on conducting media. The closest topic deals with thin layer cells, usually incorporated as part of an integrated circuit. Unfortunately, very little can be adopted from the techniques used in these cases since they usually encompass micrometer thick layers, with solid electrolyte in between, that simplifies greatly the production method (in particular the requirement for pinhole-free, intimate contact between the two active materials thin films).

In the current study, both films were deposited by vacuum thermal evaporation, one of the simplest thin layer deposition methods. The as-deposited films were amorphous, oxygen-deficient and cover the Pt-foil substrate quite homogeneously over large areas (Figures S1 and S2 in the Supporting Information (SI)). However, in order to obtain the specific crystalline phases in which we are interested, the as-deposited V_2O_5 and the MoO_3 films have to be "annealed" after deposition. The latter stage ensures that the films will assume the right stoichiometry (re-oxidation) and the desired crystallographic phase. This stage is also accompanied by morphology changes. The latter is usually undesirable, as it usually leads to crystallites growth and island formation, leading to a partially exposed underlayer (Figure S1 in the SI). While such a morphology is tolerable in single layer studies, it is inadequate for discrete bilayers experiments.

Based on previous studies, we first established the best conditions for the deposition of single monolithic thin layers of V_2O_5 and MoO_3 on Pt foils, as well the best effective ways to analyze the results. The study concentrated on the thermal deposition parameters and postdeposition treatments. With both materials, the crucial end-point was to obtain thin layers of the materials with the appropriate crystallographic structures. This was ascertained by XRD, Raman spectroscopy, HR-SEM +EDS, and AFM although, by far, the most sensitive analytical technique was based on electrochemical measurements, particular SSRCV. Despite its inherent simplicity, it provides very accurate information regarding the mass load, oxidation state, purity, and crystal structure of the deposits. Each of the materials and their byproducts (e.g., VO_2, amorphous and partially crystalline V_2O_5, etc.) show particular and well recognized electrochemical response.

The physical properties of the materials, in general, and the electrochemical characteristics in particular, are strongly determined by the crystal structure of the given material. Hence, in the next step, we studied the parameters affecting the bilayer properties, in particular, the crystalline structure and texture of each of the single phases. Initially, the crystal structures and textures of the polycrystalline Pt (p-Pt) plated MoO_3/V_2O_5 and V_2O_5/MoO_3 electrodes were determined via XRD and were compared with the MoO_3 and V_2O_5 monolayer thin film electrodes.

Figure 1 compares the XRD pattern for MoO_3/V_2O_5, V_2O_5/MoO_3, MoO_3, and V_2O_5 electrodes, all deposited on Pt foils. The diffraction pattern of the V_2O_5 film deposited on Pt corresponds to an orthorhombic (α) phase with unit cell parameters of a = 11.48 Å, b = 4.36 Å, and c = 3.55 Å. The crystalline monolayers V_2O_5 are apparently possess partially preferential orientation along the (010) plane.

The monolayered MoO_3 patterns correspond to orthorhombic (α) phase with clear preferentially oriented (010) planes and unit cell parameters of a = 3.95 Å, b = 13.8 Å, and c = 3.69 Å.

Very different results were obtained for a thin layer of MoO_3 deposited on top of a V_2O_5 layer. As an upper layer in the bilayered structure, it exhibits markedly different texture and crystallinity. New peaks were observed in the diffraction pattern of MoO_3/V_2O_5 at 2θ = 23.06° and 25.1° that can be indexed to the (011) and (200) planes of the monoclinic (β) phase of MoO_3, respectively. The new peak at 2θ = 23.4° is associated with the α-phase and can be indexed to the (−1−10) plane.

Analyzing the XRD patterns of the V_2O_5/MoO_3 bilayer reveals that the crystal structure of the V_2O_5 deposited on top of a MoO_3 layer is the same as that for V_2O_5 deposited directly on Pt. However, the (−3−10) peak has completely vanished, and

DOI: 10.1021/acs.jpcc.9b04371
J. Phys. Chem. C 2019, 123, 16577−16587

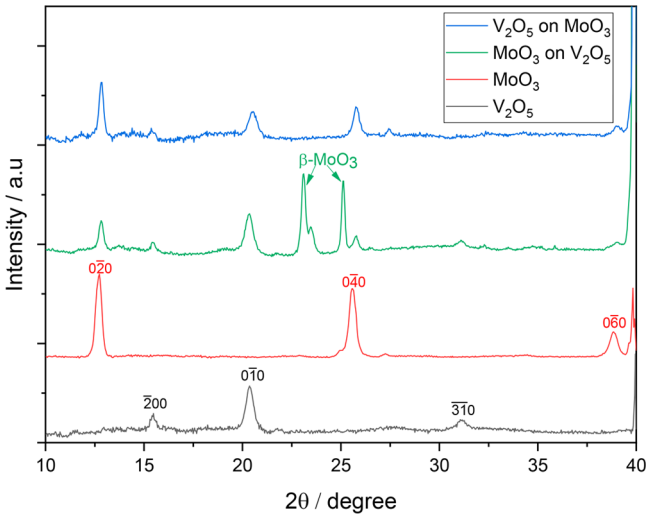

Figure 1. XRD patterns of monolithic V_2O_5, MoO_3, V_2O_5/MoO_3, and MoO_3/V_2O_5 thin film electrodes deposited onto polycrystalline Pt foil.

the ratio between the (0−10) and (−200) peaks increased. This indicates that the V_2O_5 grown on top of α-MoO_3 assumes a higher proportion of preferential (010) plane orientation perpendicular/horizontal to the surface plane.

Raman spectroscopy was used to investigate some chemical and structural attributes for these complex model systems. Figure 2a shows the Raman spectra of MoO_3/V_2O_5, V_2O_5/MoO_3, MoO_3, and V_2O_5 electrodes, all deposited on p-Pt foil.

The single V_2O_5 layer spectra exhibit the characteristic peaks located at 285, 305, 406, 482, 529, 704, and 995 cm^{-1} associated with the stretching modes of α-V_2O_5 with orthorhombic unit cell.[31] Figure 2c compares the Raman spectra of V_2O_5 and V_2O_5/MoO_3. In accordance with the XRD results, the Raman spectrum supports the conclusion that the crystal structure of the V_2O_5 remains unaltered in both systems. However, it can be discerned that the peaks of V_2O_5 in the V_2O_5/MoO_3 bilayer system are broader than those for the V_2O_5 single layer on Pt alone. This suggests that there is a small, but not zero, effect of the substrate, Pt vs MoO_3, on the crystallite size, strain, or presence of structural defects and possibly morphology of V_2O_5. This will be further addressed later in the paper.

The MoO_3 Raman peaks at 665, 820, and 995 cm^{-1} are associated with the α orthorhombic phase of MoO_3.[32] As can be seen from Figure 2b, new peaks at 776, 850, and 900 cm^{-1} are observed alongside the characteristic peaks of the pure α-phase, when the MoO_3 is deposited on top of V_2O_5. These new peaks are typical for a β-monoclinic phase of MoO_3.[32] These results are consistent with the existence of a mixture of the two phases when the MoO_3 is deposited on top of V_2O_5. In contrast, pure α orthorhombic MoO_3 is obtained when the oxide is deposited directly on p-Pt.

From Raman and XRD analyses, we can deduce that the crystalline structure and the preferential ordering of the deposited materials, especially MoO_3, are highly affected by the substrate. In the case of MoO_3, the orthorhombic crystal structure with perfect (010) orientation changed to a mixture of two phases (β + α) and the perfect orientation is disrupted when changing the substrate from Pt to V_2O_5. The crystalline structure of the V_2O_5 is less sensitive to the substrate, while the crystallite growth yields an appreciably more preferentially oriented deposit when the V_2O_5 is deposited on top of the 010 oriented MoO_3 layer.

Morphology and Elemental Analysis. The morphology of the active materials frequently has a profound impact on the electrochemical performance of a given intercalation compound. This is particularly true for explicitly structured electrode materials architectures (thin monolithic films, coated and core−shell electrode materials).

The morphology and particle size distribution of the upper layer metal oxides was studied by HR-SEM and AFM. Before

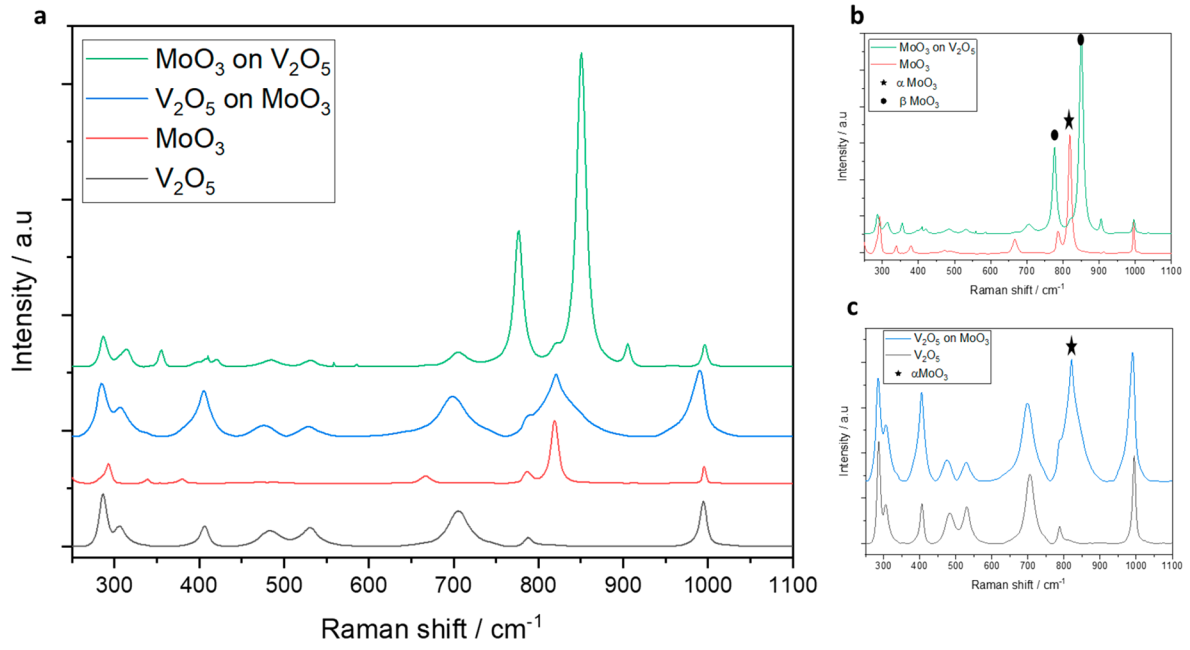

Figure 2. (a) Raman spectra of monolithic V_2O_5, MoO_3, V_2O_5/MoO_3, and MoO_3/V_2O_5 thin film electrodes deposited on polycrystalline Pt. (b,c) Comparative Raman spectra of (b) MoO_3 and (c) V_2O_5 thin layers grown on clean, polycrystalline Pt and on top of the other metal oxide, respectively. Stars designate peaks associated with the α-phase of MoO_3, and dots with β phase of MoO_3.

DOI: 10.1021/acs.jpcc.9b04371
J. Phys. Chem. C 2019, 123, 16577−16587

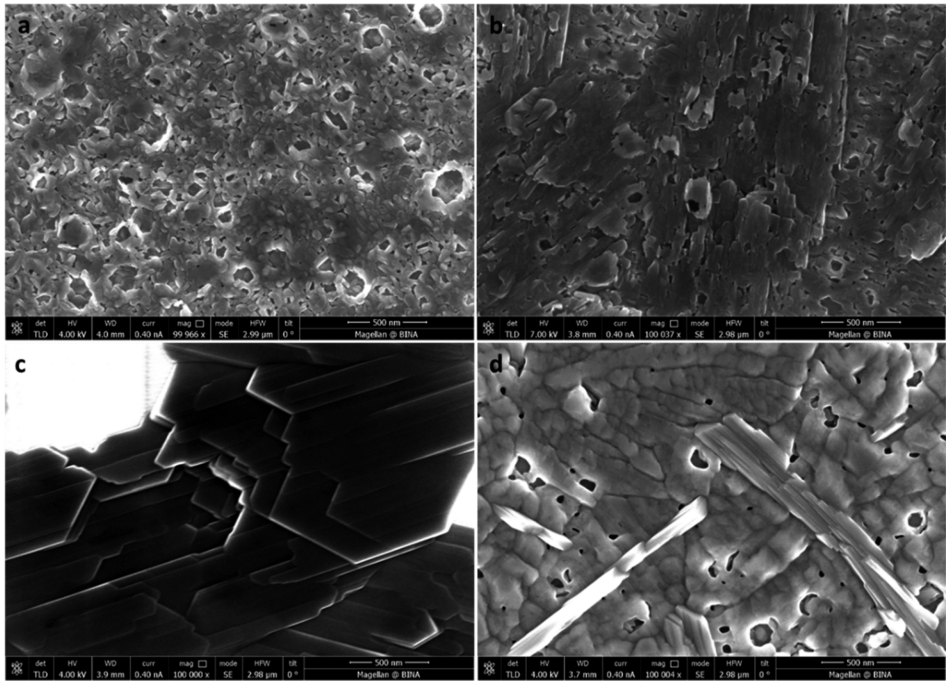

Figure 3. HR-SEM images of monolithic (a) V_2O_5, (b) V_2O_5/ MoO_3, (c) MoO_3, and (d) MoO_3/ V_2O_5 thin films electrodes (on polycrystalline Pt) at 100K magnification.

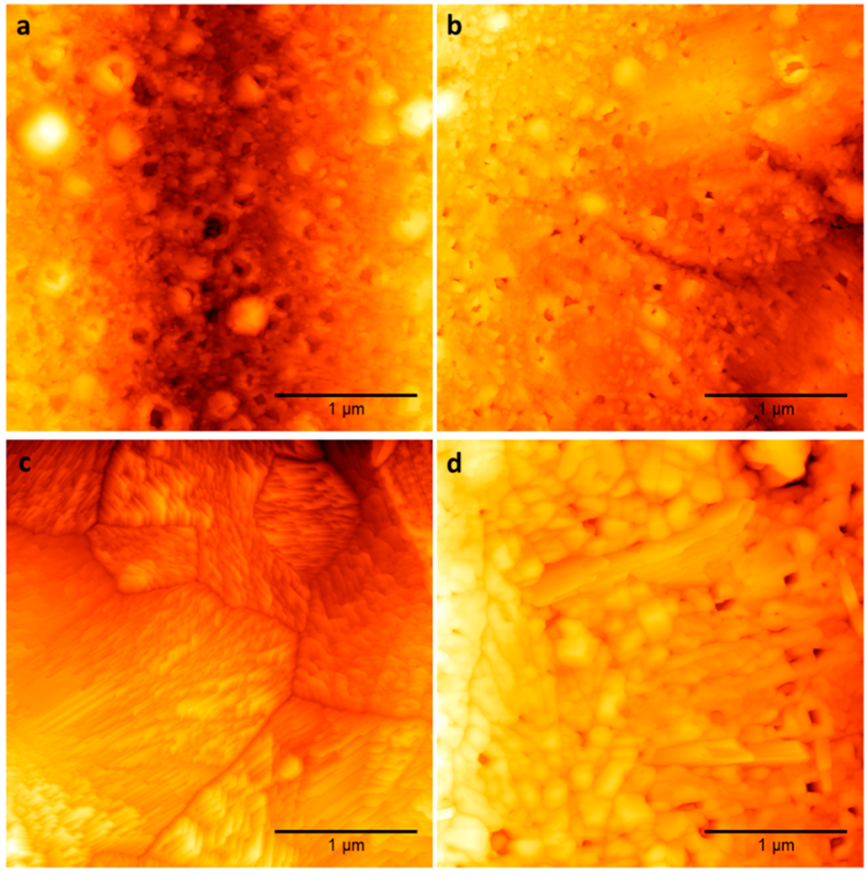

Figure 4. AFM images of the monolithic (a) V_2O_5, (b) V_2O_5/MoO_3, (c) MoO_3, and (d) MoO_3/V_2O_5 thin film electrodes (on polycrystalline Pt) at 20K magnification.

elaborating on intricate morphology attributes of the films, we studied the surface coverage and density of the deposits under low magnification. It was found that V_2O_5 deposits form pretty full coverage across the entire substrate, even after "annealing" (Figures S1 and S3 in the SI). On the other hand, under the current experimental conditions, the as-deposited MoO_3 forms

DOI: 10.1021/acs.jpcc.9b04371
J. Phys. Chem. C 2019, 123, 16577−16587

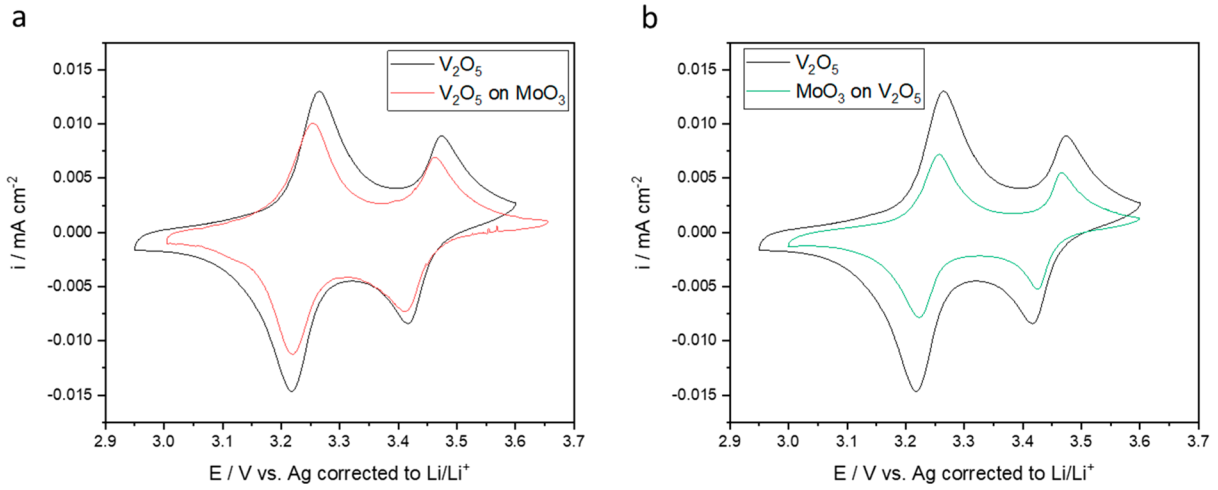

Figure 5. Comparative CV curves for V_2O_5 and (a) V_2O_5/MoO_3, (b) MoO_3/V_2O_5 thin film electrodes over a potential range in which only V_2O_5 is electrochemically active and undergoes highly reversible $\alpha \rightarrow \varepsilon \rightarrow \delta$ phase transitions.

an amorphous, dense fully covered substrate. On annealing, the single-layer oxide segregates into large crystals with poor substrate coverage (Figures S1 and S3 in the SI). This behavior completely changes when the substrate is changed to polycrystalline V_2O_5, in this case, large-area, continuous coverage of film forms. This reveals that the film growth mode is highly substrate dependent.

HR-SEM and AFM images of MoO_3/V_2O_5, V_2O_5/MoO_3, MoO_3, and V_2O_5 electrodes are presented in Figures 3 and 4, respectively. As can be seen from Figures 3a,b, and 4a,b, there is a moderate difference in the morphology of the V_2O_5 film, depending on the substrate. It is important to note that the few micrographs presented constitute a carefully selected set of images, from a very large number of micrographs, that, to the best of our ability, present typical views, rather than unique, outlier cases.

The morphology of the thin V_2O_5 film is characterized by small (~50 nm) and randomly oriented crystals when it is deposited directly on p-Pt under the experimental conditions. Interestingly, changing the substrate only, in the case of V_2O_5 coated on crystalline MoO_3, the V_2O_5 crystals are now appreciably larger (>500 nm) and show a higher degree of preferential orientation. It is important to note that the underlying MoO_3 films, as noted before, are nonuniform, covering only separated islands of the material on the Pt substrate. Thus, in this case, the effect of the MoO_3 as a substrate on the V_2O_5 layer was examined only on selected sections covered with sufficiently large areas of MoO_3 layers (see EDAX spectra at Figure 7 in the SI).

In contrast to the case of V_2O_5 on MoO_3 bilayers, MoO_3 coated onto crystalline α-V_2O_5 exhibited remarkable modifications. Both of the deposits' crystalline structure, layer morphology, and surface coverage of the MoO_3 were significantly altered by the change in the substrate. Figures 3c,d and 4c,d present HR-SEM and AFM images of MoO_3 and MoO_3/V_2O_5 thin film electrodes, respectively. The micrographs reveal that the MoO_3 deposited on microcrystalline Pt yields large, perfect crystals, around 3 μm across, with an apparent layered structure. Most importantly, the HR-SEM images of MoO_3/V_2O_5exhibit a ruglike deposit of smaller, elongated, densely packed grains with no visual evidence for a layered structure. The most important feature of the MoO_3 on V_2O_5 bilayer is the complete coverage of the electrode, nearly pinhole-free, across the entire electrode surface. Apparently, the wetting and adhesion of MoO_3 to V_2O_5 is good and results in full, continuous coverage. These results open a door for better understanding of the interplay between the substrates, experimental conditions, and layer structures. It provides a protocol for the synthesis of a dense, monolithic thin film of MoO_3, over large areas, by thermal deposition. A quest considered as very difficult.

In the following section, we show how these crystallographic and morphological differences are reflected by the electrochemical properties the films.

Electrochemical Analysis. Electrochemical measurements have the benefit of being extremely sensitive, i.e., materials and processes specific. In many cases, the specificity of the electrochemical response and its sensitivity exceed those of high-end analytical techniques, such as XPS, XRD, and EDS. Using the correct electrochemical technique and careful analysis of the results may shed light on the physical, electrochemical, structural, and morphological properties of the tested material. Cyclic voltammetry (CV) is one of the most commonly used electroanalytical techniques. It is frequently utilized for the study of new materials' properties, such as those mentioned above. Interesting and valuable scientific insights can be provided by associating the materials properties (structure and morphology) with their electrochemical response. We studied the various samples' electrochemical responses by CV, after establishing the optimal setup and conditions, like scan rate, solutions chemistry, and so forth.

Figure 5 presents the first CV curves for the monolithic V_2O_5, V_2O_5/MoO_3, and MoO_3/V_2O_5 thin film electrodes over a narrow potential region, within which only the orthorhombic α-V_2O_5 is electrochemically active and undergoes the highly reversible, two sequential 1/2 e^- (and two 1/2 Li^+ insertions) and $\alpha \rightarrow \varepsilon \rightarrow \delta$ phase transitions.[30,31,33,34] As can be clearly observed, all the CVs exhibit this, well documented, electrochemical response. This provides strong evidence that neither the substrate nor the overlayer has a significant effect on the crystal structure of electroactive V_2O_5. These results are consisted with the Raman and XRD results.

Figure 5a compares the CV curves for V_2O_5 and V_2O_5/MoO_3 electrodes. The single-layer V_2O_5 exhibits higher current densities than those of V_2O_5/MoO_3. These results can be explained by two plausible mechanisms. One based on

DOI: 10.1021/acs.jpcc.9b04371
J. Phys. Chem. C 2019, 123, 16577−16587

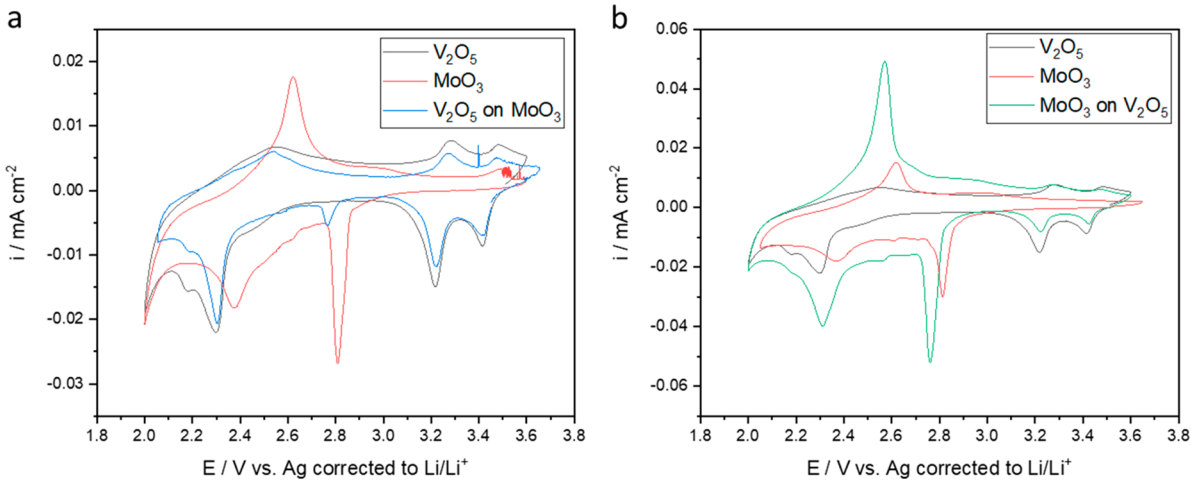

Figure 6. CV curves for single layers of V_2O_5 and MoO_3 compared to (a) V_2O_5/MoO_3 and (b) MoO_3/V_2O_5 thin film electrodes in three electrodes cell, over a wide potential range in which both MoO_3 and V_2O_5 are electrochemically active.

electronic conductivity and the other on morphology grounds: (1) In the case of V_2O_5/MoO_3 electrodes, the MoO_3, over the experiment's potential window, serves solely as the electron conducting mediator (current collector, CC) between the electroactive compound (V_2O_5) and the underlying current collector (Pt). Now, since MoO_3 is a poor electronic conductor, the intercalation kinetics of V_2O_5 deposited directly on Pt is faster than that of V_2O_5 on MoO_3. (2) Morphology has a substantial influence on intercalation kinetics. As was noted above, the annealed V_2O_5 layer deposited directly on p-Pt exhibits substantially smaller particle size than that deposited on MoO_3. Smaller particles mean shorter solid-state diffusion distance as well as larger surface area, characteristics which may lead to better intercalation kinetics. It definitely may be that both mechanisms are responsible for the differences in the electrochemical response for this structured system.

In addition, regarding the V_2O_5/MoO_3 structured samples, since the coverage of the first layer, the annealed MoO_3, on the Pt substrate is poor, it is important to stress that these electrodes represent a mixed response of V_2O_5 plated directly on p-Pt and V_2O_5 on the MoO_3 underlayer. Hence, it is also possible that only the V_2O_5 sections plated directly on Pt are fully active, while those plated on MoO_3 are kinetically impeded. This may explain the smaller charges associated with the CVs.

Figure 5b shows the first/steady state CV curves of V_2O_5 and MoO_3/V_2O_5 electrodes. Here, as in the previous case, the single-layer V_2O_5 electrodes deliver higher charge per mass (higher specific intercalation capacity) and exhibit higher current densities than those of the bilayer MoO_3/V_2O electrodes. In this case, a simple and plausible explanation involves the isolating property of the outer MoO_3 layer. The V_2O_5 layer in the current case is covered by a dense and compact layer of MoO_3, which impedes ion transport from the solution. An interesting question arises from these results: Is the electrochemical response of the V_2O_5 as an underlayer substantially weaker? Microscopy measurements (low and high magnifications, and EDS data) indicate that the MoO_3 layer, in this case, is quite homogeneous and compact over the entire electrode. In the potential window of the CVs, MoO_3 is inactive. As it is Li-free, it cannot simply act as a Li ion conductor. Taking all these into consideration, there is an open question as to how Li ions pass through the MoO_3 "interphase", allowing a substantial part of the underlayer V_2O_5 to intercalate reversibly Li ions. Obviously, it might be that, despite the high-resolution microscopy visual inspections, the MoO_3 layer is actually much more porous that seen visually, leaving Li ions passage channels. A less probable, but intriguing possibility is that the MoO_3 thin layer has the capability to transport Li ions across its crystalline structure by a mechanism, akin to solid-state ion conductors, yet to be studied. For instance, although far-fetched, it could be that, by Donnan equilibrium with the Li ion rich solution, a small amount of Li ions spontaneously inserts into the oxide, thereby imparting the material Li ion conductivity. This question, however, is beyond the scope of this study.

Interestingly, in both bilayered electrodes, one can observe a small but recurring trend in the voltage separation for each of the two coupled redox peaks. In both cases, the redox peak separation for the single layer V_2O_5 is larger than that for the bilayers. Specifically, for the V_2O_5 single layer, the peak separation for the $\alpha \rightarrow \varepsilon$ and $\varepsilon \rightarrow \delta$ couples are 54 and 50 mV, respectively. For MoO_3/V_2O_5 and V_2O_5/MoO_3, the values are around 44 and 35 mV for the $\alpha \rightarrow \varepsilon$ and $\varepsilon \rightarrow \delta$ phase transitions, respectively. The peak potential separation may shed light on the electrochemical reversibility of these systems (from charge transfer kinetic point of view). As the peak separation is smaller, the charge transfer kinetics and the reversibility of the electrochemical process are better. The apparent improved kinetics in the bilayer structures may be due to preferential orientation of V_2O_5 particles which may facilitate the intercalation process in the case of the V_2O_5/MoO_3 system. For the MoO_3/V_2O_5 system, the improved kinetics, compared to the single layer V_2O_5, may be related to the formation of new solid−solid interphase which facilitates ion transfer across it.

Figure 6 presents the first CV cycle for monolithic V_2O_5, MoO_3, V_2O_5/MoO_3, and MoO_3/V_2O_5 thin film electrodes over a wider potential region, in which both compounds are electrochemically active. Since scanning the voltages to lower than 2.3 V vs Li is associated with irreversible materials phase transformations, only the first cycle is considered in this study. In all cases, V_2O_5, initially undergoes the two 1/2 e^- per unit reversible intercalations described above. When the voltage scan drops below 2.3 V vs Li, a strong and sharp reduction peak appears, followed by a smaller, wavelike one, at ca. 2.18 V vs Li. This well documented electrochemical response is associated

DOI: 10.1021/acs.jpcc.9b04371
J. Phys. Chem. C 2019, 123, 16577−16587

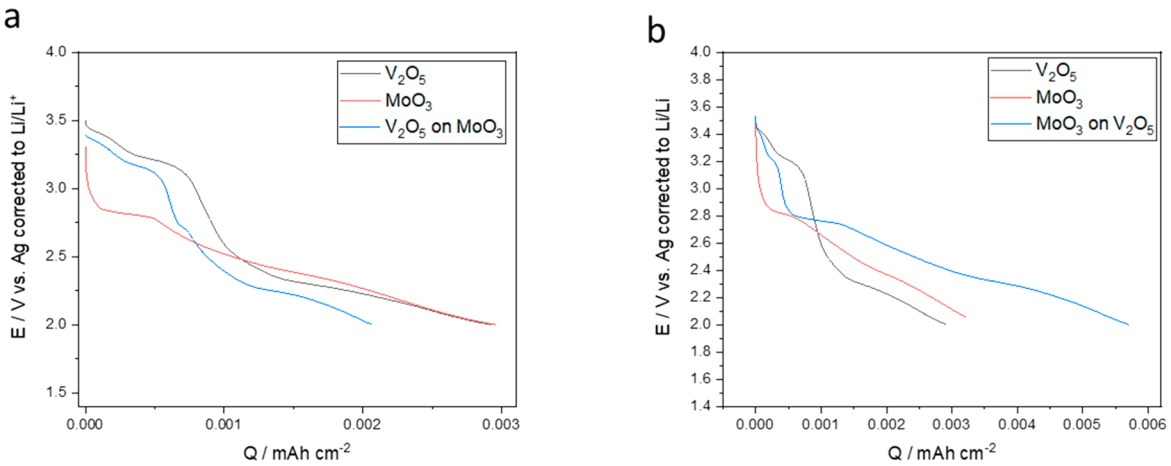

Figure 7. Potential vs discharge specific capacity curves of V_2O_5 and MoO_3 compared to (a) V_2O_5/MoO_3 and (b) MoO_3/V_2O_5 thin film electrodes calculated by numerical integration of the CV curves represented in Figure 6 using EC-lab software.

with the irreversible $\delta \rightarrow \gamma$ phase transition.[31,33,34] The positive scan follows the known deintercalation curve, with a broad oxidation peak centered at 2.5 V vs Li. In the first cycle, one can see the two, now broadened, 1/2 Li^+ deintercalation peaks, at 3.27 and 3.48 V vs Li, associated with now partially deformed $\delta \rightarrow \varepsilon \rightarrow \alpha$ phase transitions. Further cycling wipes out these distinct peaks to a single, wide, unstructured one.

The electrochemical response of the single layer MoO_3 also corresponds well to its documented Li intercalation and phase transitions.[29,35] The sharp and strong reduction peak at around 2.8 V vs Li/Li^+ and the capacity associated with it are typical to Li ion intercalation into the crystalline MoO_3. For V_2O_5/MoO_3 electrode all MoO_3 response peaks are very small, although the mass loads of MoO_3 in the two experiments (single layer MoO_3 and V_2O_5/MoO_3 bilayer electrodes) are practically identical. Thus, in contrast to V_2O_5, MoO_3 becomes practically electrochemically inactive as an inner layer in the bilayer electrodes. The electrochemical response of the upper V_2O_5 layer is qualitatively similar to that of the single layer material. Quantitatively, the charges associated with its CV curve are somewhat lower, although the mass load of V_2O_5 is practically identical in the two experiments. These results are consistent with almost complete blocking/isolation of MoO_3 from solution's ions access by V_2O_5. The electrochemical response of the V_2O_5 layer is consistent with its "normal" behavior, suggesting that most of the material, which is deposited directly on the Pt CC, behaves, as expected, as a single-layer electrode. The smaller capacities probably reflect the portion of the V_2O_5 mass load deposited on the small portions of the CC covered by the large MoO_3 crystals.

In the case of MoO_3/V_2O_5 electrodes, one can see that the charge associated with the V_2O_5 peaks (3.2, 3.4, 2.3 V vs Li/Li^+) is appreciably smaller (ca. one-half) than that with a single V_2O_5 layer. Interestingly, the strong electrochemical response of the upper, MoO_3 layer unveils the significant impact of the substrate on the electrochemical activity of the material. The MoO_3 shows much improved electrochemical activity when deposited on V_2O_5. The improved performance is manifested by higher current densities and higher charges associated with the intercalation and deintercalation of Li. These interesting results are probably due to the better MoO_3 deposition morphology on V_2O_5 compared with Pt. the MoO_3 layer grown on V_2O_5 shows complete coverage. Thus, for the same mass load, this translates to a much thinner film. Consequently, the MoO_3 layer on V_2O_5 is constituted of much smaller crystallites (shorter diffusion length) and a much larger surface area. Additionally, the deposit morphology suggests that the wetting of MoO_3 is significantly better on V_2O_5 than on Pt, leading also to better adherence and better electrical contact with the CC.

The good electrochemical response for MoO_3 on V_2O_5 reveals another, not less important, fact. Since in this case the V_2O_5 the first layer coverage is completed and homogeneous, the MoO_3 upper layer activity attests that the under-layer possesses sufficiently high electronic conductivity, allowing electrons percolation to the MoO_3. This property is of great importance for bilayer architecture electrodes that utilizing transition metal compounds.

Interestingly, there is a peculiar response for MoO_3 in the two double layered structured electrodes compared with the single layer on Pt. In Figure 6, one can observe that the peak at ca. 2.8 V vs Li shifts to lower potential of around 2.75 V vs Li in the bilayer electrode. In Figure 6b, it is easy to see that the two other peaks, at 2.38 and 2.62 V vs Li, also shift to lower potentials at the same magnitude. Since all peaks shift in the same direction this cannot be attributed to *iR* drops or kinetic limitations. It is possible that the RE value and the *X*-axis post measurement calibration causes this shift, and, thus, it is erroneous. However, any other RE value calibration will cause the V_2O_5 peaks to exhibit potential shift, of the same magnitude, in the opposite direction. This will constitute equally peculiar observation. At the current stage, we have no simple and logically coherent explanation for this phenomenon.

In order to describe quantitatively the effect of integrating the tested materials into complex structures on the charge stored by them, we present in Figure 7 potential vs capacity (E vs Q) curves. The data was calculated using numerical integration of the voltammetric curves (E as a function of I vs t, along the voltammograms). It would be interesting and important to discuss herein aspects of volumetric and gravimetric specific capacities and specific energies since materials for cathodes in rechargeable batteries are involved. However, the core focus of this study was not issues related to materials' performance, but rather understanding the interactions and interrelations in two layer structures (between the layers) and their influence on important electrochemical intercalation processes. Consequently, we provide graphs of E vs charge/cm^2 for the processes we explored, which seem to provide useful responses of them.

DOI: 10.1021/acs.jpcc.9b04371
J. Phys. Chem. C 2019, 123, 16577−16587

Figure 7a shows the E vs Q curves of the V_2O_5, MoO_3, and V_2O_5/MoO_3 electrodes calculated from the CV curves shown in Figure 6a. The first and the most noticeable observation is that the double layered V_2O_5/MoO_3 structure possesses smaller discharge capacity by 33% than that of each of the single-layered electrodes. This means that engineering of such core−shell, coating, or double layered structure composed of an inner core of MoO_3 and outer shell of V_2O_5 is not suitable for energy storage systems. V_2O_5 and V_2O_5/MoO_3 show two plateaus around 3.4 and 3.2 V vs Li related to the CV peaks corresponding to the $\alpha \rightarrow \varepsilon$ and $\varepsilon \rightarrow \delta$ phase transition, respectively. It is noticeable that the single layer V_2O_5 electrode delivers a higher amount of charge compared to the double layer V_2O_5/MoO_3 electrode via lithium intercalation involves these phase transitions. Actually, the capacity loss of the V_2O_5 in the V_2O_5/MoO_3 structure is around 30% compared to the single layered V_2O_5 electrode. As mentioned above, the coverage of the inner MoO_3 layer is also around 30%, indicating that the V_2O_5 deposited on MoO_3 is practically inactive electrochemically. In addition, the MoO_3 E vs Q curve shows a plateau at 2.8 V vs Li corresponding to the phase transition of MoO_3 during Li intercalation into it. This plateau is almost not obtainable in the V_2O_5/MoO_3 E vs Q curve, which indicates that the MoO_3 is electrochemically inactive in this double layered configuration.

Figure 7b shows the E vs Q curves of the V_2O_5, MoO_3, and MoO_3/V_2O_5 electrodes calculated from the CV curves shown in Figure 6b. In this case, the MoO_3/V_2O_5 electrodes deliver a specific capacity of 0.0057 mAh cm^{-2} which is in approximately the sum of the specific capacities delivered by each of the single layered V_2O_5 and MoO_3 electrodes. The plateau at 3.2 V vs Li, present in the E vs Q curves of the V_2O_5 and MoO_3/V_2O_5 electrodes, indicates that only around 50% of the inner V_2O_5 is active in the MoO_3/V_2O_5 electrodes. In addition, higher charge is delivered in the process around 2.8 V vs Li (corresponding to the phase transition of MoO_3) with the MoO_3/V_2O_5 electrodes, compared to the charge involved the process with the single layered MoO_3 electrodes. These results indicate that the improved capacity of the MoO_3/V_2O_5 double layered structure compared to each of the single layered electrodes is mainly due to the effect of the substrate on the physical properties of the MoO_3, as explained above. In addition, unlike the case of the V_2O_5/MoO_3, electrodes, the MoO_3 $/V_2O_5$ structure enables both layers to be electrochemically active in the composite (be-layered) electrodes.

It is important to note, again, that microscopy measurements with V_2O_5/MoO_3 and MoO_3/V_2O_5 indicated that the outer layer fully covers the bottom one with what seems to be a dense deposit. The intercalation process into the inner material can be understood based on two different grounds. It might be that, despite the indications from the microscopy measurements, the upper layer is porous, to a greater or lower extent. Another possibility is that the upper layer transports Li ions from the solution to the inner one by solid-state mass transport mechanisms akin to solid-state solutions.

The first proposition is simple and straightforward, although, obviously, it constitutes an experimental inadequacy of the sample preparation stages for the purposes of this study. The second possibility can be relatively simply understood in cases where the intercalation compound constituting the upper layer complies with two essential characteristics: (A) The material must first contain Li ions. (B) The chemical potential between the two layers should favor Li ion transfer through the interphase.

Regarding case (A), with these intercalation compounds, this might happen under two circumstances: (1) Some (extremely low) spontaneous Li ion insertion as a result of a contact equilibrium between the high Li ion concentrated solution and the Li-free compound. (Some spontaneous Li intercalation might also happen in the case where the intercalation compound reacts directly with oxidation-prone solution species and contaminants by redox reaction.) (2) By electrochemical intercalation. This depends on the electrochemical window under which the experiment is carried out. As to case (B), this depends on the redox potential of the intercalation compounds and the intercalation level as determined by the biasing voltage.

CONCLUSIONS

The effect of combining different materials in complex structures on their physical and electrochemical properties was studied. The physical characterizations of the films were focused on crystallographic aspects of the thin films, which were afforded by combination of Raman spectroscopy, XRD, and electrochemical measurements. Comprehensive electrochemical characterizations were used also to furnish additional qualitative and quantitative data.

For this study, we made use of simple, geometric (macroscopic area, nanometer-scale thickness, 2D bilayers) model systems. These were tailored as monolithic MoO_3 and V_2O_5 bilayers. The thin films were carefully constructed to be of well-documented Li intercalation compounds, possessing the appropriate characteristics to perform well as additive-free, pure compounds. In such a way, we could afford studying pure, monolithic intercalation materials without the need for the common additives (e.g., binders, conducting additives). These constitute excellent model systems for an in-depth study of electrons and ion transport playing in intercalation mechanisms and electrochemistry of double-layered active materials.

It has been revealed that some of the physical properties of thin crystalline layers of MoO_3 and V_2O_5, e.g., crystalline structure and morphology, are strongly affected by the substrates on which they are deposited. These differences strongly affect the materials' electrochemical characteristics.

In this study, we found that the morphology, texture, and crystal structure of MoO_3 had significantly transformed when it was deposited on a layer of microcrystalline α-V_2O_5 in contrast to microcrystalline Pt. Such changes are predicted to occur also in the case of microscopic or nanometric core−shell particles, where such effects are notoriously harder to identify. When deposited on p-Pt, MoO_3 appears as an orthorhombic, α-MoO_3 phase, with a perfect (010) orientation. This is transformed to a mixture of two phases, β and α, when the deposition was carried out on polycrystalline, thin α-V_2O_5 film. The deposited layer in this case lacked a preferred orientation.

In general, the crystal structure of the deposited V_2O_5 was found to be insensitive to the substrate nature. Both on p-Pt and on microcrystalline α-MoO_3, V_2O_5 crystallized in the α-phase. There was a difference in the degree of the preferential orientations, with randomly and 010 on p-Pt and α-MoO_3, respectively. Interestingly, significant morphological changes had been clearly observed. Such morphology changes sometimes lead to dramatic effects on the physical and electrochemical properties of such thin films.

It is not unexpected that thin film structures will be affected by the substrate, among other deposition parameters. Indeed, in

DOI: 10.1021/acs.jpcc.9b04371
J. Phys. Chem. C 2019, 123, 16577−16587

both cases, the morphology of the upper deposit was found to be determined by the lower one. The MoO_3 changed from large, easily visible perfect crystals with layered structure on p-Pt to ruglike deposits of smaller, elongated, densely packed grains on α-V_2O_5. The morphology of the thin V_2O_5 film on p-Pt was characterized by small (~50 nm) and randomly oriented crystals. When deposited on α-MoO_3, much larger crystallites grew (>500 nm), with a higher degree of preferential orientation.

In terms of electrochemical characteristics, the two inverse structures show marked differences. The V_2O_5/MoO_3 bilayer electrodes yielded 33% lower specific capacity compared to each of the single-layered, single-phase electrodes. In addition, the capacity associated with V_2O_5 solely, within the V_2O_5/MoO_3 structure, is around 70% of that of pure V_2O_5. Based in the voltammetric response, it can be reasonably deduced that practically only V_2O_5 was electrochemically active, while MoO_3 was essentially inert.

On the contrary, the MoO_3/V_2O_5 electrodes exhibited only around 5% less charge than the sum of the capacities of the individual components as single layers. It had been shown, though, that the MoO_3 outer layer capacity was larger than that when the material was deposited on p-Pt. This phenomenon is in line with the significantly better surface morphology of the MoO_3 when deposited on V_2O_5.

In addition to intercalation capacities, the two different, inverse structures showed also marked changes associated with intercalation kinetics. Although this delicate point has to be studied in greater detail, preliminary conclusions could be suggested based on peak separations in the CV curves. In essence, the intercalation of Li ions into V_2O_5 showed better kinetics in both cases of V_2O_5/MoO_3 composites compared to pure V_2O_5 on p-Pt.

The two inverse structures suggest that dramatically different properties may be attained by bilayer engineered composites, such as core−shell particles, depending on the nature of the inner and outer layers.

Modulation of physical characteristics of such materials may have great significance in a variety of materials science studies, e.g., electrochemical sensors, actuators, energy conversion and accumulation, and catalysis, as well as in photonics and photoactive components.

In particular, such, and other, materials' properties alterations are of utmost importance in the ever-increasing scientific activity associated with core−shell active electrochemical materials for battery applications. Such property modifications will eventually influence the ability of the materials to serve as parts of complex configuration electrode materials. In this paper, we have shown that the electrochemical performance, in terms of kinetics, thermodynamics, phase transitions, reversibility, and specific capacity may be strongly modified when assembling materials into complex architectures. This study sheds light on some of the critical factors which have to be taken into account when engineering new, composite electrode materials.

■ ASSOCIATED CONTENT

Supporting Information

The Supporting Information is available free of charge on the ACS Publications website at DOI: 10.1021/acs.jpcc.9b04371.

HR-SEM images of monolithic MoO_3 and V_2O_5 thin film electrodes (on polycrystalline Pt) before and after annealing; Raman spectra of monolithic MoO_3 and V_2O_5 thin film electrodes (on polycrystalline Pt) before and annealing; HR-SEM images of the monolithic V_2O_5, MoO_3, V_2O_5 on MoO_3 and MoO_3 on V_2O_5 thin film electrodes at 20K magnification; HR-SEM image and the corresponding EDAX spectra of V_2O_5 thin film electrode; HR-SEM image and the corresponding EDAX spectra of MoO_3 thin film electrode; HR-SEM image and the corresponding EDAX spectra of MoO_3/V_2O_5 thin film electrode; HR-SEM image and the corresponding EDAX spectra of V_2O_5/MoO_3 thin film electrode (PDF)

■ AUTHOR INFORMATION

Corresponding Authors

*E-mail: raniatiias@gmail.com.
*E-mail: Doron.Aurbach@biu.ac.il.

ORCID

Ran Attias: 0000-0003-0528-7664
Michael Salama: 0000-0002-3495-2822

Notes

The authors declare no competing financial interest.

■ ACKNOWLEDGMENTS

Partial support for this project was obtained from the EC Horizon 2020 program (E-Magic consortium) and by the INREP project supported by the Israeli Committee of High Education.

■ REFERENCES

(1) Yin, Z.; Ding, Y.; Zheng, Q.; Guan, L. CuO/Polypyrrole Core − Shell Nanocomposites as Anode Materials for Lithium-Ion Batteries. *Electrochem. Commun.* **2012**, *20*, 40−43.

(2) Kim, H.; Cho, J. Superior Lithium Electroactive Mesoporous Si@ Carbon Core−Shell Nanowires for Lithium Battery Anode Material. *Nano Lett.* **2008**, *8*, 3688−3691.

(3) Liao, J.; Higgins, D.; Lui, G.; Chabot, V.; Xiao, X.; Chen, Z. Multifunctional TiO 2 − C/MnO 2 Core−Double-Shell Nanowire Arrays as High-Performance 3D Electrodes for Lithium Ion Batteries. *Nano Lett.* **2013**, *13*, 5467−5473.

(4) Sun, B.; Chen, Z.; Kim, H.; Ahn, H.; Wang, G. MnO/C Core − Shell Nanorods as High Capacity Anode Materials for Lithium-Ion Batteries. *J. Power Sources* **2011**, *196*, 3346−3349.

(5) Su, L.; Jing, Y.; Zhou, Z. Li Ion Battery Materials with Core−Shell Nanostructures. *Nanoscale* **2011**, *3*, 3967.

(6) Ren, M. M.; Zhou, Z.; Gao, X. P.; Peng, W. X.; Wei, J. P. Core−Shell Li 3 V 2 (PO 4) 3 @C Composites as Cathode Materials for Lithium-Ion Batteries. *J. Phys. Chem. C* **2008**, *112*, 5689−5693.

(7) Li, Y.; Qian, F.; Xiang, J.; Lieber, C. M. Nanowire Electronic and Optoelectronic Devices. *Mater. Today* **2006**, *9*, 18−27.

(8) Cui, L.-F.; Ruffo, R.; Chan, C. K.; Peng, H.; Cui, Y. Crystalline-Amorphous Core−Shell Silicon Nanowires for High Capacity and High Current Battery Electrodes. *Nano Lett.* **2009**, *9*, 491−495.

(9) Jian, Z.; Liu, P.; Li, F.; He, P.; Guo, X.; Chen, M.; Zhou, H. Core-Shell-Structured CNT@RuO 2 Composite as a High-Performance Cathode Catalyst for Rechargeable Li-O 2 Batteries. *Angew. Chem., Int. Ed.* **2014**, *53*, 442−446.

(10) Maliakal, A.; Katz, H.; Cotts, P. M.; Subramoney, S.; Mirau, P. Inorganic Oxide Core, Polymer Shell Nanocomposite as a High K Gate Dielectric for Flexible Electronics Applications. *J. Am. Chem. Soc.* **2005**, *127*, 14655−14662.

(11) Velikov, K. P.; Moroz, A.; van Blaaderen, A. Photonic Crystals of Core-Shell Colloidal Particles. *Appl. Phys. Lett.* **2002**, *80*, 49−51.

(12) Ivanov, S. A.; Piryatinski, A.; Nanda, J.; Tretiak, S.; Zavadil, K. R.; Wallace, W. O.; Werder, D.; Klimov, V. I. Type-II Core/Shell CdS/

DOI: 10.1021/acs.jpcc.9b04371
J. Phys. Chem. C 2019, 123, 16577−16587

ZnSe Nanocrystals: Synthesis, Electronic Structures, and Spectroscopic Properties. *J. Am. Chem. Soc.* **2007**, *129*, 11708−11719.
(13) Graf, C.; van Blaaderen, A. Metallodielectric Colloidal Core−Shell Particles for Photonic Applications. *Langmuir* **2002**, *18*, 524−534.
(14) Wu, F.; Chen, J.; Chen, R.; Wu, S.; Li, L.; Chen, S.; Zhao, T. Sulfur/Polythiophene with a Core/Shell Structure: Synthesis and Electrochemical Properties of the Cathode for Rechargeable Lithium Batteries. *J. Phys. Chem. C* **2011**, *115*, 6057−6063.
(15) Cui, L.-F.; Yang, Y.; Hsu, C.; Cui, Y. Carbon−Silicon Core−Shell Nanowires as High Capacity Electrode for Lithium Ion Batteries. *Nano Lett.* **2009**, *9*, 3370−3374.
(16) Duan, W.; Zhu, Z.; Li, H.; Hu, Z.; Zhang, K.; Cheng, F.; Chen, J. Na 3 V 2 (PO 4) 3 @C Core−Shell Nanocomposites for Rechargeable Sodium-Ion Batteries. *J. Mater. Chem. A* **2014**, *2*, 8668−8675.
(17) Li, C.; Zhang, H. P.; Fu, L. J.; Liu, H.; Wu, Y. P.; Rahm, E.; Holze, R.; Wu, H. Q. Cathode Materials Modified by Surface Coating for Lithium Ion Batteries. *Electrochim. Acta* **2006**, *51*, 3872−3883.
(18) Ohta, N.; Takada, K.; Sakaguchi, I.; Zhang, L.; Ma, R.; Fukuda, K.; Osada, M.; Sasaki, T. LiNbO3-Coated LiCoO2 as Cathode Material for All Solid-State Lithium Secondary Batteries. *Electrochem. Commun.* **2007**, *9*, 1486−1490.
(19) Cho, J.; Kim, Y. J.; Park, B. Novel LiCoO 2 Cathode Material with Al 2 O 3 Coating for a Li Ion Cell. *Chem. Mater.* **2000**, *12*, 3788−3791.
(20) Sun, Y.-K.; Lee, Y.-S.; Yoshio, M.; Amine, K. Synthesis and Electrochemical Properties of ZnO-Coated LiNi[Sub 0.5]Mn[Sub 1.5]O[Sub 4] Spinel as 5 V Cathode Material for Lithium Secondary Batteries. *Electrochem. Solid-State Lett.* **2002**, *5*, A99.
(21) Breen, M. L.; Dinsmore, A. D.; Pink, R. H.; Qadri, S. B.; Ratna, B. R. Sonochemically Produced ZnS-Coated Polystyrene Core−Shell Particles for Use in Photonic Crystals. *Langmuir* **2001**, *17*, 903−907.
(22) Xie, J.; Tong, L.; Su, L.; Xu, Y.; Wang, L.; Wang, Y. Core-Shell Yolk-Shell Si@C@Void@C Nanohybrids as Advanced Lithium Ion Battery Anodes with Good Electronic Conductivity and Corrosion Resistance. *J. Power Sources* **2017**, *342*, 529−536.
(23) Su, L.; Jing, Y.; Zhou, Z. Li Ion Battery Materials with Core-Shell Nanostructures. *Nanoscale* **2011**, *3*, 3967−3983.
(24) Son, S. B.; Gao, T.; Harvey, S. P.; Steirer, K. X.; Stokes, A.; Norman, A.; Wang, C.; Cresce, A.; Xu, K.; Ban, C. An Artificial Interphase Enables Reversible Magnesium Chemistry in Carbonate Electrolytes. *Nat. Chem.* **2018**, *10*, 532−539.
(25) Menkin, S.; Golodnitsky, D.; Peled, E. Artificial Solid-Electrolyte Interphase (SEI) for Improved Cycleability and Safety of Lithium-Ion Cells for EV Applications. *Electrochem. Commun.* **2009**, *11*, 1789−1791.
(26) Attias, R.; Salama, M.; Hirsch, B.; Goffer, Y.; Aurbach, D. Anode-Electrolyte Interfaces in Secondary Magnesium Batteries. *Joule* **2019**, *3*, 27−52.
(27) Luo, W.; Lin, C. F.; Zhao, O.; Noked, M.; Zhang, Y.; Rubloff, G. W.; Hu, L. Ultrathin Surface Coating Enables the Stable Sodium Metal Anode. *Adv. Energy Mater.* **2017**, *7*, 1−6.
(28) Li, N. W.; Yin, Y. X.; Yang, C. P.; Guo, Y. G. An Artificial Solid Electrolyte Interphase Layer for Stable Lithium Metal Anodes. *Adv. Mater.* **2016**, *28*, 1853−1858.
(29) Gershinsky, G.; Yoo, H. D.; Gofer, Y.; Aurbach, D. Electrochemical and Spectroscopic Analysis of Mg^{2+} Intercalation into Thin Film Electrodes of Layered Oxides: V_2O_5 and MoO_3. *Langmuir* **2013**, *29*, 10964−10972.
(30) Attias, R.; Salama, M.; Hirsch, B.; Pant, R.; Gofer, Y.; Aurbach, D. Anion Effects on Cathode Electrochemical Activity in Rechargeable Magnesium Batteries: A Case Study of V2O5. *ACS Energy Lett.* **2019**, *4*, 209−214.
(31) Attias, R.; Salama, M.; Hirsch, B.; Gofer, Y.; Aurbach, D. Solvent Effects on the Reversible Intercalation of Magnesium-Ions into V2O5 Electrodes. *ChemElectroChem* **2018**, *5*, 3514−3524.
(32) Diaz-Droguett, D. E.; El Far, R.; Fuenzalida, V. M.; Cabrera, A. L. In Situ-Raman Studies on Thermally Induced Structural Changes of Porous MoO 3 Prepared in Vapor Phase under He and H 2. *Mater. Chem. Phys.* **2012**, *134*, 631−638.
(33) Meulenkamp, E. A.; Van Klinken, W.; Schlatmann, A. R. In-Situ X-Ray Diffraction of Li Intercalation in Sol-Gel V2O5films. *Solid State Ionics* **1999**, *126*, 235−244.
(34) Li, Y.; Yao, J.; Uchaker, E.; Yang, J.; Huang, Y.; Zhang, M.; Cao, G. Leaf-Like V 2 O 5 Nanosheets Fabricated by a Facile Green Approach as High Energy Cathode Material for Lithium-Ion Batteries. *Adv. Energy Mater.* **2013**, *3*, 1171−1175.
(35) Swiatowska-Mrowiecka, J.; de Diesbach, S.; Maurice, V.; Zanna, S.; Klein, L.; Briand, E.; Vickridge, I.; Marcus, P. Li-Ion Intercalation in Thermal Oxide Thin Films of MoO3 as Studied by XPS, RBS, and NRA. *J. Phys. Chem. C* **2008**, *112*, 11050−11058.

DOI: 10.1021/acs.jpcc.9b04371
J. Phys. Chem. C 2019, 123, 16577−16587